Control system optimization techniques for real-time applications in fusion plasmas: the RFX-mod experience

L. Pigatto, M. Baruzzo, P. Bettini, T. Bolzonella, G. Manduchi, G. Marchiori

***Abstract*—A series of techniques are presented that have been developed to optimize the output magnetic field of the feedback control system on the RFX-mod reversed field pinch device. With the aim of minimizing the harmonic distortion and correcting localized error fields, these methods should be lightweight for real-time application and effective in improving the performance of a system that is routinely used for active control of magneto-hydro-dynamic plasma instabilities. The implementation of simple, linear algebra based, real-time optimization methods will be described along with proof of the sought beneficial effects. Focus of the work is set on a spurious harmonics reduction technique based on the decoupling of sensors and actuators, a description of its derivation will be given together with the implementation in the control loop. A similar procedure for the compensation of faulted actuators will also be mentioned.**

I. Introduction

MAGNETIC confinement of fusion relevant plasmas is the target of many devices that are nowadays working towards the achievement of electricity from controlled fusion reactions. Such plasmas constitute a particularly harsh nuclear environment in which violent instabilities can arise, causing confinement losses and possible damage to structural materials. Effective control of such instabilities is therefore compulsory for controlled fusion experiments, with active control playing an important role. The RFX-mod experiment is a medium size (R = 2 m, a = 0.459 m) toroidal device that has been operating since 2004. Originally designed as a Reversed-Field-Pinch experiment [1], it is capable of confining plasmas also in the Tokamak configuration [2]. It is equipped with a state-of-the-art system for active control of magneto-hydro-dynamic (MHD) instabilities [3]. Such a system, operating with a cycle frequency from 2.5 to 5 kHz, is composed of 192 independently fed actuators (saddle coils arranged into a 4×48 grid), located on the outer surface of a stainless steel support structure at r=0.6 m, and a considerable set of magnetic sensors counting 192 bi-axial pick-up probes (measuring toroidal and poloidal B components) and 192 saddle sensors for the radial component [4] . Each active coil can be fed a maximum current of 400 A, providing a DC radial field of 46 mT at the vacuum vessel surface. The radial component of the magnetic field in particular, is measured by 192 saddle probes whose positions correspond to the projection of the actuators on the outer surface of the vacuum vessel, at minor radius r=0.505 m. The high degree of flexibility of the control system, working in a bi-dimensional Fourier space characterized by the poloidal (m) and toroidal (n) mode numbers, allows to switch on or off each single coil. Many control schemes can thus be easily implemented [5] and the controller has the capacity to independently act on selected modes with different sets of coils. In order to improve the efficiency and effectiveness of the active control system, a series of efforts have been made in optimizing the produced magnetic fields, for example by minimizing the harmonic distortion due to the toroidal geometry, or adapting the control scheme to real experimental conditions, such as the fault of one or more sparse active coils [6]. The techniques used to achieve these results, which will be illustrated in the present work, have been tested both in simulations and experiment. A dynamic simulator has been developed for the purpose of testing optimization strategies [7]. It consists of a detailed three-dimensional description of the conducting structures coupled to a two-dimensional plasma magneto-hydro-dynamic (MHD) model. These are the two components of the CarMa code [8] [9] which is then integrated by a complete representation of the real time control system.

L. Pigatto is with Università degli Studi di Padova, Padova, Italy and Consorzio RFX, Corso Stati Uniti, 4 35127, Padova, Italy (e-mail: leonardo.pigatto@igi.cnr.it).

M. Baruzzo is with Consorzio RFX, Corso Stati Uniti, 4 35127, Padova, Italy.

P. Bettini is with Università degli Studi di Padova, Padova, Italy and Consorzio RFX, Corso Stati Uniti, 4 35127, Padova, Italy.

T. Bolzonella is with Consorzio RFX, Corso Stati Uniti, 4 35127, Padova, Italy.

G. Manduchi is with Consorzio RFX, Corso Stati Uniti, 4 35127, Padova, Italy.

G. Marchiori is with Consorzio RFX, Corso Stati Uniti, 4 35127, Padova, Italy.

II. The Coupling Problem

Improving the performance of the control system described in Section I is a complicated task that can be tackled by using the coupling terms between actuators and sensors. Given the presence of passive structures in between, these coupling terms are frequency dependent. Decoupling based optimization techniques have been developed with different concepts, such as the so-called dynamic decoupler [10] which relies on offline pre-computed current distributions. In the present work we will concentrate on a different, lightweight method that can be applied real-time taking action on all the modes of the Fourier spectrum for a fixed frequency. Dedicated measuring campaigns have been carried out on RFX-mod, leading to the development of a full electromagnetic model of the MHD modes active control system [11]. Mutual coupling matrices between active coils can be derived for a given set of frequencies from the ratio between coil voltage ($\bar{V}_i$) and coil current

($\bar{I}_k$) phasors. The resulting complex number can account for the effects of passive structures on the magnetic flux.

$$\frac{\bar{V}_i(\omega)}{\bar{I}_k(\omega)} = \dot{Z}_{ik}(\omega) = R_{ik} + j\omega\dot{L}_{ik}(\omega) \tag{1}$$

The same procedure can be followed to measure the coupling terms between actuators and sensors, only changing the voltage phasor with the flux measured by each saddle sensor.

$$\frac{\bar{\Phi}_i(\omega)}{\bar{I}_k(\omega)} = \dot{M}_{ik}(\omega) \tag{2}$$

Once the response of the saddle sensors has been measured for the desired frequencies, full information on mutual couplings can be used to build a full state-space electromagnetic model. This *black-box* model derived from experimental data can be used to develop simplified strategies for improving the quality of harmonic content in output magnetic fields, taking into account the effect of toroidal geometry and coil-sensor couplings. Another way to proceed in challenging the decoupling problem, is making use of existing three-dimensional electromagnetic codes to obtain a first-principles description of the coils and passive structures. This has been done for the RFX-mod device with the CARIDDI code. From this second model, which will be described in Section III, another state-space representation of the system is obtained from which the following transfer function can be calculated:

$$K(\omega) = \left[C(j\omega - A)^{-1}B + D\right] \tag{3}$$

where standard state-space notation is considered with the matrices A, B, C, D. By inverting the transfer function $K(\omega)$ for a given frequency, a matrix is obtained that can be used to account for the couplings and reduce the magnetic field harmonic distortion. Various matrices have been obtained with both the aforementioned methods and applied in simulations (details on the simulation tools are given is Section III) and experiments. Some examples of these matrices are reported in Figure 1, from which the different magnitude of coupling can be appreciated with varying frequency and between experimental or model based calculations. Figure 1a and 1b represent the decoupling matrices obtained from experimental data for $\omega = 0, 10$ Hz, while Figure 1c is the inverse of the CarMa transfer function in the infinite frequency limit. This latter particular case is also called *D-matrix*, since it is calculated from the only surviving part of Eq.3 after the $\omega \to \infty$ limit. All these matrices are normalized to their maximum value and they will be used, as specified in Section III, to recombine the current reference pattern fed to active coils.

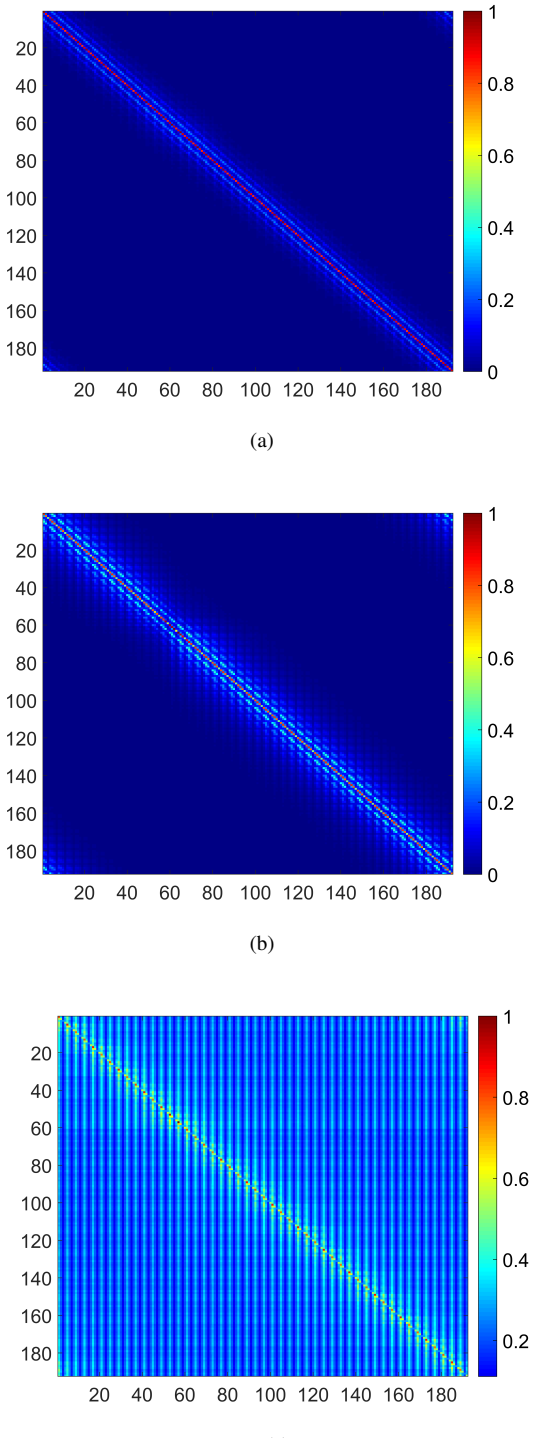

Fig. 1. (a) Experimental decoupling matrix calculated for $\omega = 0$, i.e. step-like request. (b) Experimental decoupling matrix calculated for $\omega = 10Hz$. (c) CarMa derived decoupling matrix representing the infinite frequency limit. All matrices are normalized to their maximum value (Please refer to the online version of the paper for the colors).

III. The Model

A. Dynamic simulation tool-set

A dynamic simulator has been developed as a Matlab Simulink application to allow the simulation of a full control loop and the test of the optimization techniques described in the present paper. The core of this flight simulator is a state-space representation of the system (Plant) given by the CarMa code, which is integrated with a complete representation of the digital control system. This allows for a realistic description of the passive and active structures with the effects of 3D geometry on plasma dynamics. The active system can be simulated at its full potential or downgraded to a reduced number of coils with virtually any geometry. The CarMa code itself is the result of coupling a 3D eddy current problem

integral solution (given by the CARIDDI code) with a 2D linearized MHD solution, which results from the MARS-F code [12]. Instantaneous plasma response to a given perturbation is calculated on a coupling surface (S) and used to evaluate the effect of the 3D structures on the plasma. The currents induced by the plasma in these structures are computed using an equivalent surface current distribution on S, such that it generates the same magnetic field as the plasma just outside S. The model used for the dynamic simulator in particular, includes a fully 3D description of the resistive copper shell surrounding the vacuum vessel (3 mm thick with $\tau_V = 50$ ms vertical field penetration time) as well as including the active system components. The copper shell itself is the fundamental component in plasma stability applications, since it slows down to its characteristic penetration time some of the fastest growing MHD instabilities (i.e. ideal kinks),thus allowing the possibility of feedback control [13]. The flexibility of the RFX-mod digital controller allows to apply different control strategies, the most common one being the so-called clean-mode-control (CMC) [14]. This method consists in acting independently on each harmonic component of the discrete Fourier transform of the radial magnetic field. Furthermore a real-time algorithm is applied to remove the aliasing error from the magnetic field harmonic component measurement, caused by high order sidebands produced by the 4×48 discrete grid of active saddle coils. A block scheme of the system described above is given in Figure 2, both for the open-loop case (Figure 2a, in which the sidebands cleaning is not applied) and closed-loop (Figure 2b). An exploded diagram of the control system block can be seen in Figure 2c, in which the application of the decoupling based on static matrices is represented, as described in Section II. The main part of the Plant block is the state-space representation of the CarMa model, which is implicitly preceded by the saddle coil current controller. Finally a state-space filter has been added to the Plant block, also in series with the main model, in order to mimic the effect of the stainless steel vacuum vessel, with a 5 ms time constant.

B. Validation of the vacuum model

The main goal to be achieved with the optimization procedures described here is the correct assessment of the system external action on a given plasma. In order to do so, all the experimental sessions dedicated to the evaluation of mutual couplings have been carried out in vacuum. The same has been done for the modeling activity, a vacuum version of the CarMa model has been used and benchmarked against experimental data in terms of harmonic content of the output magnetic field. The very good agreement of simulated B field amplitude and current with experimental data can be appreciated in Figure 3. During this open-loop vacuum shot the active system has been requested a particular perturbation with n=1 and m=-6 mode numbers. The same shot can be reproduced as a dynamic simulation. The amplitude of the $(1, -6)$ component of the output field is shown for both cases in Figure 3a, where the *raw* data is used, indicating that the sideband cleaning procedure has not been applied for the particular case. Figure 3b shows the current $(1, -6)$ harmonic component, confirming that the

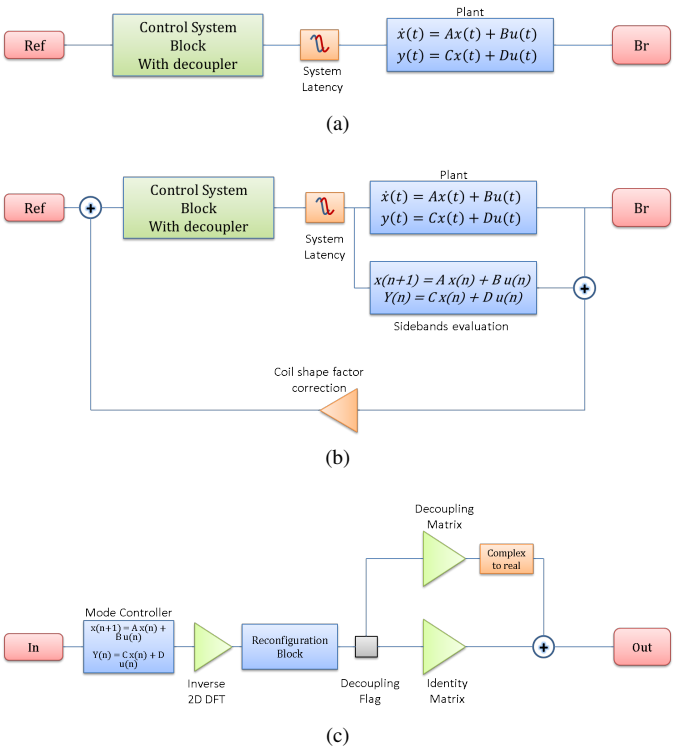

Fig. 2. (a) Open loop diagram. (b) Closed loop diagram with clean-mode-control. (c) Exploded control system block with decoupler.

developed simulation tools can successfully represent the real vacuum experimental setup. Figure 3 is not only showing the general agreement between simulation and measurements but also the capability of the software tools of reproducing a very peculiar configuration. Specifically, during shot 33863 a reduced coil array has been implemented, with the $(1, -6)$ magnetic perturbation generated by only 12 active coils along the outermost toroidal array. This leaves a characteristic pattern in the produced sidebands which can be appreciated in Figure 4. The amplitude of each harmonic is given in the bar-plot, normalized to the desired $(1, -6)$, at a given time instant of the flat-top phase. The harmonic pattern is given by the peculiar periodicity of the active array and it is correctly reproduced by the open-loop simulation.

IV. Open loop operation with decoupling matrices

The first set of matrices generated from both experimental measurements (as described in Section II) and the CarMa code (Section III) has been applied for the open-loop generation of magnetic field perturbations of varying amplitude and phase. The Total Harmonic Distortion of the output fields has been used in order to evaluate the effectiveness in spurious harmonics reduction.

$$THD = \frac{\sum_i B_i^2 - B_{target}^2}{B_{target}^2} \tag{4}$$

where the index i runs on all the harmonic components of the field signal. An example of this total harmonic distortion analyses is reported in Figure 5, in which two different decoupling strategies have been used for the generation of a

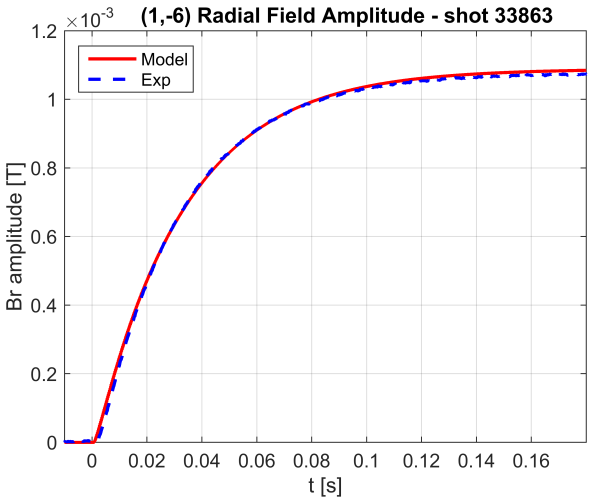

(a)

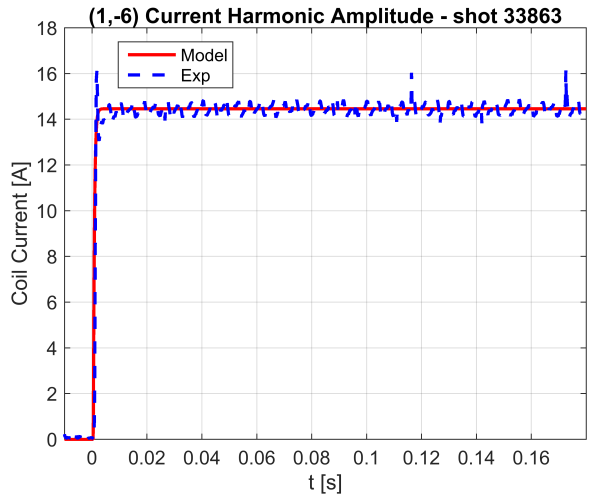

(b)

Fig. 3. Experimental and model time evolution of m=1, n=-6 harmonic component of the radial field (raw) (a) and saddle coil currents (b). Simulation and data from shot 33863.

step-like perturbation. The red dashed line shows the reduction of spurious harmonic content when the specific model-derived matrix is used, with respect to the blue solid line (identity matrix, i.e. no decoupling applied). The green dotted line shows a degradation of the harmonic content instead, this is due to the peculiar applied matrix, obtained through an infinite frequency limit from Eq.3. Because of this limit, the so-called *D matrix* does not work well for a step-like request during the steady phase. On the other hand its effect can be appreciated during the fast transient phase, as in Figure 5b, when the B field is increasing rapidly and the infinite frequency limit holds, during the first 30 ms in particular. The smaller harmonic distortion obtained with a given decoupling matrix is reflected in the amplitude of the B field spurious harmonics, this can be appreciated for two different cases in Figure 6. For the step-like magnetic perturbation (Figure 6a) a simple decoupling matrix helps in reducing the amplitude of the $(m = 0, n = 6)$ component, the very same result has been obtained in dedicated vacuum experiments [15].

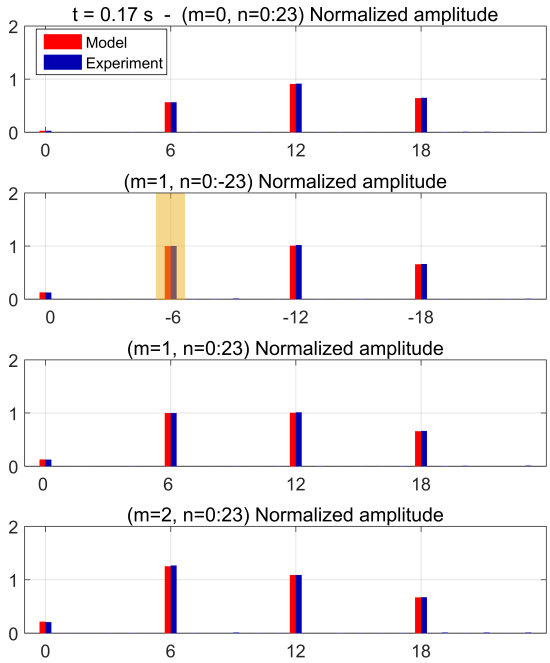

Fig. 4. Comparison between model and experiment relative harmonic content of the radial magnetic field (raw) in shot 33863. Amplitudes taken in steady phase at t=0.17 s

Another matrix has been used with the dynamic simulator for a 10 Hz perturbation, resulting in a reduced spurious harmonics relative content (Figure 6b). It should be noted that the matrices applied in the aforementioned reference cases (represented respectively in Figure 1a and 1b) are providing the best correction during the steady phase of the perturbation, while during the fast transients the infinite frequency limit holds as previously discussed.

V. Closed loop decoupling application and missing coil compensation

Once the exact behavior of the active system has been assessed by generating open-loop perturbations, the same can be done within the feedback loop. While the results to be expected are still related to reducing the harmonic pollution during steady phases, attention should also be paid to the possible gain changes introduced by recombining the reference current distribution. The static matrix shown in Figure 1a has been included in the feedback loop during dedicated experiments, allowing the verification of expected effects and validation of the modeling results. Figure 7 shows the amplitude of a $(m = 1, n = -6)$ perturbation together with its poloidal sidebands. A reduction of the $m = 0$ component is found with the non-diagonal decoupling matrix. Furthermore, since the amplitude of the requested $n = -6$ component is the same in both cases, the gain substantial invariance with application of this particular decoupling matrix can be acknowledged. The importance of this last matter lies in the fact that no change in the gain matrix has to be made if decoupling has to be switched

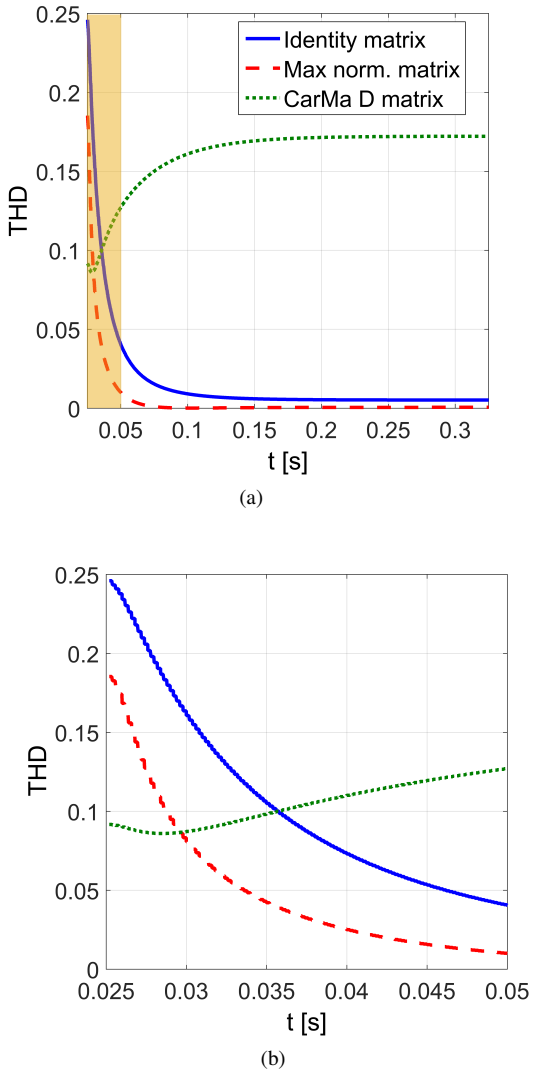

Fig. 5. (a) Total harmonic distortion from simulations with D matrix, $\omega = 0$ Hz matrix and identity matrix. (b) Zoom of the first 50 ms of the transient phase in which the effect of the D matrix, i.e. infinite frequency limit, can be appreciated. Amplitudes are normalized to the $(1, -6)$ component.

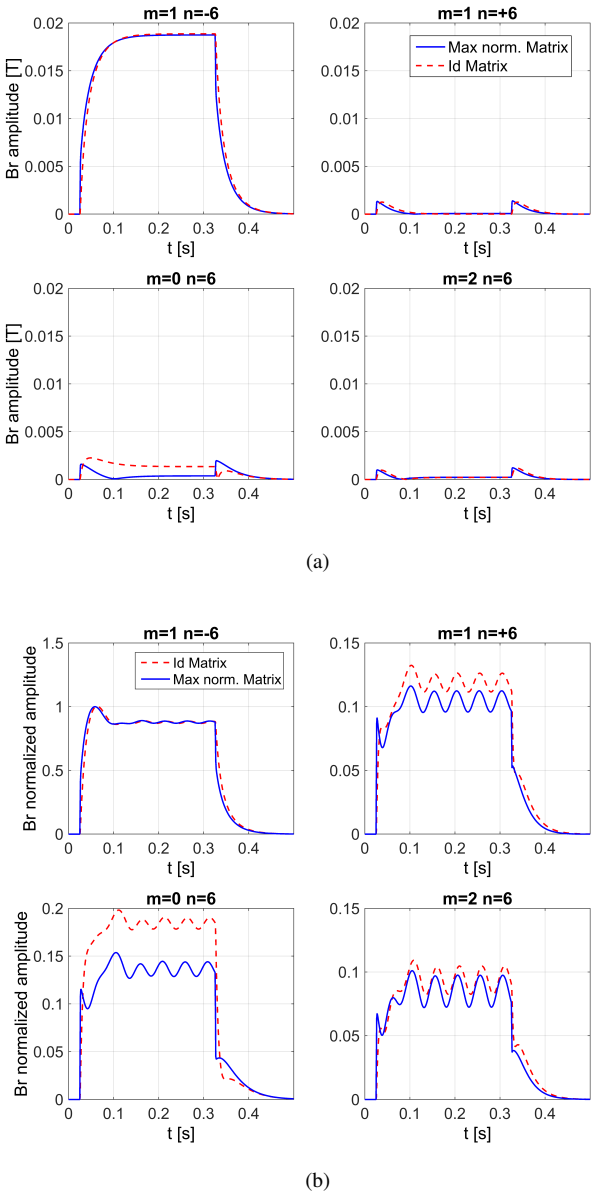

Fig. 6. Poloidal harmonics produced for $(1, -6)$ reference. (a) Step-like perturbation with no decoupling (dashed red) and with CarMa $\omega = 0$ Hz matrix applied (solid blue). (b) For a 10 Hz perturbation the dedicated decoupler is compared with the identity matrix case. As expected the decoupling effect can be appreciated in the reduction of the $(0, 6)$ and $(1, +6)$ amplitudes, in this case a normalization to the maximum of the requested harmonic has been applied to highlight the effect.

on or off during experimental campaigns. The idea of using a static matrix to recombine the active system input current distribution has also been applied to a set of problems not strictly related to decoupling sensors and actuators. Given the possibility of implementing various active coil geometries, as mentioned in Section III-B, a systematic study has been carried out to investigate the effect of one or more faulted actuators on the produced magnetic fields. This has led to the development of a set of matrices that while still aiming at the improvement of the harmonic content, are specifically designed for a system with sparse missing coils. The procedure that can be found in [6] has been proven as a simple and fast option for faulted coil compensation that allows a local reconstruction of the magnetic field and reduction of spurious harmonics.

VI. Conclusion

The present work has summarized many efforts made for the complete characterization of the RFX-mod active system in terms of output magnetic field, in particular the actuator-sensor decoupling problem has been considered. Starting from the first experimental measurements the development of simple, real-time applicable strategies to obtain almost monochromatic fields has been described. While the $(m = 1, n = -6)$ perturbation has been mainly shown in the previous sections, the same can be done for any desired B harmonic. The importance of a fast, reliable and extensively benchmarked modeling tool has to be highlighted. Each of the proposed decoupling matrices, as well as the whole missing coil compensation strategy, has been developed with full dynamic simulations before testing in dedicated experiments or implemented in

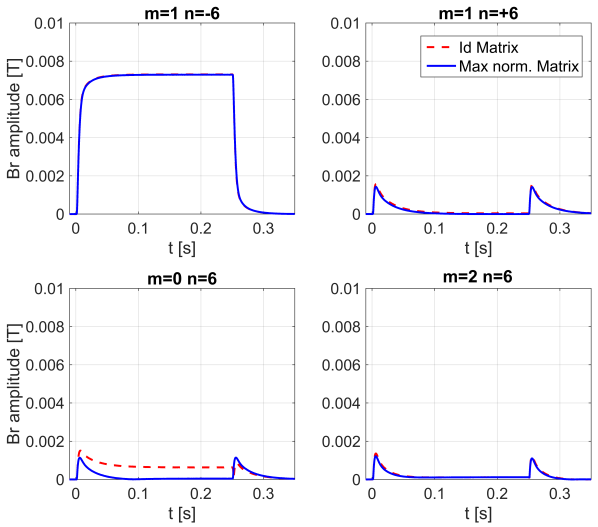

Fig. 7. Step-like $(m = 1, n = -6)$ perturbation generated in a closed-loop with purely proportional gain on the requested harmonic only. Comparison between shots 27294 and 27295.

plasma shots. The effects of actuator-sensor decoupling has thus been investigated and represented mainly by the reduction of spurious harmonics when a particular one is requested. With the introduction of the total harmonic distortion the two limiting cases, $\omega = 0$ and $\omega \to \infty$, have been identified. The high frequency behavior during transient phases has been assessed with the implementation of the so-called $D-matrix$ while two examples have been reported to show the $m = 0$ amplitude reduction when a specific decoupler is used. Finally, the closed-loop application has been reported with proof of the expected effect on the B components and of the negligible influence of the current modification on the applied gains. The concept of sparse missing coils compensation using a static matrix has been briefly mentioned.

ACKNOWLEDGMENT

This work has been carried out within the framework of the EUROfusion Consortium and has received funding from the European Unions Horizon 2020 research and innovation programme under grant agreement number 633053 and from the Italian MIUR under PRIN grant 2010SPS9B3. The views and opinions expressed herein do not necessarily reflect those of the European Commission.

REFERENCES

[1] H. Bodin and A. Newton, *Nuclear Fusion*, vol. 20, no. 10, p. 1255, 1980.
[2] J. Wesson, *Tokamaks*. Oxford University Press, 2011, vol. 149.
[3] S. Ortolani and the RFX team, *Plasma Physics and Controlled Fusion*, vol. 48, no. 12B, p. B371, 2006.
[4] P. Sonato, G. Chitarin, P. Zaccaria, F. Gnesotto, S. Ortolani, A. Buffa, M. Bagatin, W. R. Baker, S. D. Bello, P. Fiorentin, L. Grando, G. Marchiori, D. Marcuzzi, A. Masiello, S. Peruzzo, N. Pomaro, and G. Serianni, *Fusion Engineering and Design*, vol. 66-68, pp. 161–168, 2003.
[5] M. Baruzzo, T. Bolzonella, Y. Q. Liu, G. Manduchi, G. Marchiori, A. Soppelsa, M. Takechi, and F. Villone, vol. 52, no. 10, 2012.
[6] L. Pigatto, P. Bettini, T. Bolzonella, G. Marchiori, and F. Villone, *Fusion Engineering and Design*, vol. 96-97, pp. 690–693, 2015.
[7] G. Marchiori, M. Baruzzo, T. Bolzonella, Y. Q. Liu, A. Soppelsa, and F. Villone, *Nuclear Fusion*, vol. 52, no. 2, 2012.
[8] R. Albanese, Y. Q. Liu, A. Portone, G. Rubinacci, and F. Villone, vol. 44, no. 6, pp. 1654–1657, 2008.
[9] Y. Liu, M. Chu, W. Guo, F. Villone, R. Albanese, G. Ambrosino, M. Baruzzo, T. Bolzonella, I. Chapman, and A. Garofalo, *Plasma Physics and Controlled Fusion*, vol. 52, no. 10, p. 104002, 2010.
[10] L. Piron, L. Grando, G. Marchiori, L. Marrelli, P. Piovesan, A. Soppelsa, and D. Terranova, *Nuclear Fusion*, vol. 51, no. 6, p. 063012, 2011.
[11] G. Marchiori and A. Soppelsa, *Fusion Engineering and Design*, vol. 82, no. 5-14, pp. 1015–1022, 2007.
[12] Y. Liu, A. Bondeson, C. Fransson, B. Lennartson, and C. Breitholtz, *Physics of Plasmas (1994-present)*, vol. 7, no. 9, pp. 3681–3690, 2000.
[13] T. Bolzonella, M. Cavinato, E. Gaio, L. Grando, A. Luchetta, G. Manduchi, G. Marchiori, L. Marrelli, R. Paccagnella, and A. Soppelsa, *Fusion Engineering and Design*, vol. 82, no. 5, pp. 1064–1072, 2007.
[14] P. Zanca, L. Marrelli, G. Manduchi, and G. Marchiori, *Nuclear Fusion*, vol. 47, no. 11, p. 1425, 2007.
[15] L. Pigatto, P. Bettini, T. Bolzonella, G. Marchiori, and F. Villone, in *Proceedings of the 41st EPS Conference on Plasma Physics*. European Physical Society, jun 2014, p. P5.080.